Rendezvous revisited: the search for fast-intercept solutions

Eric M. Edlund

Department of Physics, SUNY Cortland

(Dated: January 24, 2023)

Abstract

It is typical of orbital interception scenarios that a chaser is actively maneuvered to intercept and rendezvous with an inertial target, which may be undertaken for a variety of purposes including docking of two spacecraft or intentional collision with an asteroid for planetary defense. Viable intercept trajectories are constrained by the free-fall path of the target and by auxiliary conditions, such as the time to intercept or the fuel budget for the chaser's intercept and rendezvous maneuvers. Whereas a constraint on the time to intercept is central to the Lambert problem, which has been studied extensively, a less common but more visually compelling constraint is a limit on the available fuel for intercept. This was the basis of a recent study [E. M. Edlund, AJP **89**, 559 (2021)], which analyzed one of two families of possible intercept solutions that were identified. The second family admits intercept at all points in the orbit and has the interesting property that it describes fast intercept solutions. This work concludes this problem by developing a general condition that describes both families of intercepts, presents representative solutions, and considers the sensitivity of these solutions to errors in the control parameter.

I. INTRODUCTION

Long before space travel was considered a possibility there was great interest in the intercept problem, first made famous by Lambert in 1761. The Lambert problem, as it is now known, seeks the velocity of a body given astronomical measurements of its position at two times because the solution allows the position to be determined at any later time, thereby providing great predictive capability. This problem spurred seminal developments in celestial mechanics and analysis by some of the best minds of the time.[1,2] There is a long and rich history of literature stemming from the Lambert problem, which was reinvigorated in the 1950's with the development of spaceflight. It lives on in modern incarnations, often with a goal of finding the thrust vector that will allow an actively maneuverable craft to intercept an inertial target (meaning a craft on a "free-fall" or "ballistic" path) at a specific time, because it is mathematically equivalent to the original problem of finding the velocity of an object given information about its position at different times. It is important to note intercept problems can be formulated with constraints other than the time-to-intercept constraint of the Lambert problem, such as intercept given a specified Δv, which can be thought of as a constraint on a quantity of fuel.

A number of recent articles have focused on interesting and insight-building problems involving orbital dynamics, including analysis of the Lambert problem using a search method,[3] using the Hohman transfer in introductory physics courses,[4] an intercept problem solved under the constraint of specified impulse,[5] an analysis of close-proximity rendezvous using the Clohesy-Wiltshire equations,[6] and a set of interesting multi-thrust methods for achieving escape velocity from an initially circular orbit.[7] Reference [5] approached the intercept problem by considering a constraint of a specified Δv, wherein it was argued that this particular variation of the intercept problem is an excellent problem for undergraduate students because the constraint on the velocity can be more readily visualized than a constraint on time and it develops deeper intuition for motion on elliptical trajectories. A simple HTML-javascript simulator provided with that article was referenced as a tool for helping to visualize and gamify this study of orbital dynamics.

While the work of Ref. [5] identified two possible families of intercept solutions, it analyzed the intercept and rendezvous problem for only the first family of solutions that occur after an integer number of orbits of the chaser. However, the second family of intercept

solutions is particularly interesting because it allows for fast intercepts that occur in less than a full orbit of the target. Such fast-intercept maneuvers are relevant to many different situations, involving existential challenges like planetary defense against civilization killing asteroids or comets where a short, but not pre-determined, time may be the essence of the problem.[8] The Planetary Defense Coordination Office, a division within NASA, tracks known threats and develops mitigation plans.[9] As part of that effort, NASA's DART mission successfully intercepted the asteroid Dimorphos, the smaller of a double-asteroid pair, on September 26 of 2022 to test deflection by kinetic impact.[10] Other applications of intercept problems include interesting developments like space debris collectors[11] and an actively maneuvering Russian satellite thought to be a satellite hunter of sorts.[12]

One can, of course, find solutions to the intercept problem using a "guess-and-check" method where initial parameters are guessed, the trajectories checked using something like the HTML-javasript program distributed with [5], and iterated until a solution is found. This approach to discovering solutions is effective but falls short of what we typically expect for a physics analysis in at least three important ways. First, such calculations necessarily rely on some other tool to plot the trajectories and therefore defers the physics analysis to someone else. Second, one quickly realizes that finding solutions using the guess-and-check approach typically requires many iterations and is not very efficient, especially if one wants to examine a range of parameters. Third, when a solution is finally realized, one has no way of determining whether it is in any way ideal or optimal without a significant effort in repeating the search process for other solutions. In contrast, an analytic solution requires greater initial effort, but also rewards with insight into the physics and provides great flexibility for exploring parameter dependency and related issues like the sensitivity of solutions to errors.

The analytical approach used here proceeds similarly to that described in Ref. [5]. The resulting condition that describes the second family of intercept locations results in a transcendental expression that is similar to analyses from diverse branches of physics, including the motion of projectiles with drag,[13] energy eigenvalues in quantum mechanics,[14,15] the structure of photonic band-gaps,[16] and the propagation of electromagnetic waves,[17] among many others. The paper proceeds with some preliminaries and a recap of important results in Section II, followed by a formal definition of the problem and derivation of the intercept condition in Section III, with discussion of solutions in Section IV. The final three sections

are brief and discuss the sensitivity of solutions in Section V, the rendezvous maneuver in Section VI, and concluding thoughts in Section VII.

II. PRELIMINARIES

The overall goal of this work is to calculate the two thrusts that are required for: (a) interception, the meeting of spacecraft, and (b) rendezvous, the matching of speeds following interception. There exist multiple methods for calculating such maneuvers. References 6 and 18 discuss a number of aspects of the intercept problem and its historical relevance. Reference 18, in particular, analyzes an intercept problem that is very similar to that discussed presently, but in the rotating reference frame of the target and using small parameter expansions.[18] The analysis presented here is different from these other analyses in that it views all motion in the inertial frame associated with the planetary mass and provides a method for exact solutions. This section begins by defining the coordinate system and initial conditions for this problem, then briefly reviews some important prior results.

A. The coordinate system and initial conditions

The analysis presented here builds on that of Ref. [5], and for the sake of continuity with that work uses the same coordinate system and symbolic representations. Figure 1 shows the coordinates used to describe the target and the chaser, the phase of the chaser's elliptical trajectory, and the two families of intercept solutions. The initial motion of both craft is taken to be in the counter-clockwise direction, which defines the sense of positive angular motion. The first family of possible intercept locations occurs at the origin of motion of the chaser and the second family exists at an angle of 2ϕ from the origin, measured in the clockwise sense. Angles in equations will be expressed in radians, whereas angles in figures will be expressed in degrees to aid with common interpretation.

The variables describing the impulse of the chaser are the magnitude of the thrust, Δv, and the thrust angle, α, which is measured in the clockwise direction from its forward motion. In the following analysis the magnitude of the thrust will often be encountered as a normalized quantity, $\delta = \Delta v / v_0$, where Δv is the change in velocity due to the first thrust maneuver and $v_0 = \sqrt{GM/r_0}$ is the orbital speed of the the target and chaser on circular

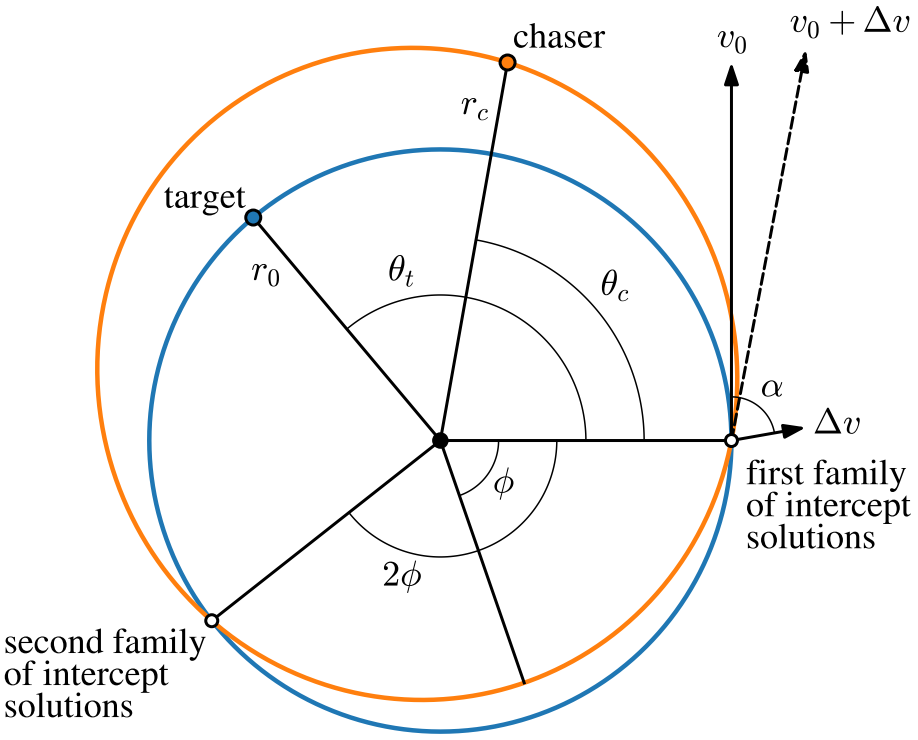

FIG. 1. The coordinate system used in this problem, showing the circular orbit of the target with radius r_0 and angular coordinate θ_t, and the elliptical orbit of the chaser with radius r_c and angular coordinate θ_c at some time t following the intercept maneuver. The angular positions of all craft are measured in the counter-clockwise direction. The phase angle of the ellipse, ϕ, is the angle of the major axis of the chaser's elliptical orbit and is measured in the clockwise sense. The initial thrust vector of the chaser is shown at the right along with the resultant velocity vector.

orbits of radius r_0, where G is the universal gravitational constant and M is the mass of the central gravitational body. A typical scale for many space missions is $\delta \approx 0.05$, but this can be greatly exceeded in special missions. For example, the third stage of the Saturn V rocket used a δ very close to the escape value of approximately 0.41, which propelled the Apollo missions from Earth orbit to the moon,[19,20] and δ's exceeding unity were achieved on the Voyager missions.

The moment immediately following completion of the chaser's intercept maneuver (engine burn) defines $t = 0$. The entire engine burn is assumed to happen over a time that effectively instantaneous, that is, so brief compared to the orbital period that the initial positions of

both craft can be taken to be those given in the following statements. Initially, the target and chaser are co-orbital on a circular trajectory, and the target remains so for all time. Using the subscript c for chaser, subscript t for target, and subscript i for initial, the initial conditions are $r_{c,i} = r_{t,i} = r_0$. The zero-reference for the angular coordinate is the position of the chaser when it initiates its intercept maneuver that is, $\theta_{c,i} = 0$. The target is initially separated from the chaser by a known angle, $\theta_{t,i} = \theta_0$, which can be positive or negative. The orbital period of the target is $T_0 = 2\pi r_0/v_0$, with orbital frequency $\omega_0 = v_0/r_0$. The engine burn of the chaser modifies its velocity by Δv directed at an angle of from the forward such that the radial and azimuthal components of the initial velocity are $v_{c,r,i} = \Delta v \sin(\alpha)$ and $v_{c,\theta,i} = v_0 + \Delta v \cos(\alpha)$, respectively.

The following discussion refers to "fast-intercept" maneuvers, which are intercepts within one orbit of the target. Two predictions for general characteristics of fast-intercept maneuvers are made. First, it seems rather intuitive that larger Δv's should result in smaller time to intercept when the optimal intercept angle is chosen. Therefore, as the impulse is increased, we anticipate that the angular coordinate at which intercept occurs should also decrease. Second, thrusts that are directed purely forward will place the chaser on an orbit with a larger period that will only increase the distance between the craft. Therefore some measure must be taken to ensure that the chaser does not drift radially outward. It follows the thrust maneuvers that are directed forward and also somewhat inward, between 270° and 360°, seem to be likely candidates for fast-intercept solutions. It is also possible that solutions with some degree of reverse thrust can place the chaser onto a lower altitude orbits that quickly advance its phase relative to the target, and therefore may also provide fast-intercept solutions. Thus, we expect that fast-intercept maneuvers will require thrust angles between 180° and 360°. These predictions will be revisited in Section IV when solutions for sample cases are presented.

B. The relationship between control parameters and ellipse parameters

Central to this work is a description of the orbital characteristics of the chaser. Following the engine burn that propels the chaser onto its intercept trajectory, it will follow an elliptical path that is described by

$$r_c(\theta_c) = r_0 \frac{1 + \epsilon \cos(\phi)}{1 + \epsilon \cos(\theta_c + \phi)}, \tag{1}$$

where ϵ is the eccentricity of the elliptical orbit and ϕ is the phase angle of the ellipse. The numerator of Eq. 1 is different from that found in many other analyses, which is typically presented as just r_0. This modified form is required so that the chaser has a radius of r_0 at $\theta_c = 0$, as required by the initial conditions.

The connection between parameters describing the ellipse, namely the eccentricity ϵ and orbital phase angle ϕ, and the control parameters, δ and α, are derived in the appendix. The results of that analysis are repeated here for convenience,

$$\epsilon = \delta \sqrt{\sin^2(\alpha)\left(1 + \delta\cos(\alpha)\right)^2 + \cos^2(\alpha)\left(2 + \delta\cos(\alpha)\right)^2}, \tag{2}$$

and

$$\tan(\phi) = \tan(\alpha)\frac{1 + \delta\cos(\alpha)}{2 + \delta\cos(\alpha)}. \tag{3}$$

Kepler's third law, describing the relationship between the orbital period and the semi-major axis of an ellipse is $T^2 = (4\pi^2/GM)a^3$, where a is the semi-major axis of the ellipse. Noting that the maximum radial excursion (apogee) occurs when $\theta_c + \phi = \pi$ and that this distance is equal to $(1+\epsilon)a$, it follows from Eq. 1 that $a = r_0(1 + \epsilon\cos(\phi))/(1 - \epsilon^2)$. This relation allows the period of the chaser's elliptical orbit to be calculated from Kepler's third law and expressed in terms of problem parameters as

$$T_c = T_0 \left(\frac{1 + \epsilon\cos(\phi)}{1 - \epsilon^2}\right)^{3/2}. \tag{4}$$

The normalized period (T/T_0) is plotted as a function of α in Fig. 2 for a range of δ. The orbital period relationship will enter the generalized intercept condition in Sec. III when accounting for the time required for the chaser to complete multiple orbits.

III. DERIVATION OF THE GENERALIZED INTERCEPT CONDITION

The full rendezvous problem can be analyzed in two parts, corresponding to the chaser's two thrust maneuvers. The first is the thrust required for interception, which is the condition that the chaser and target are coincident in space and time. The second is the thrust required

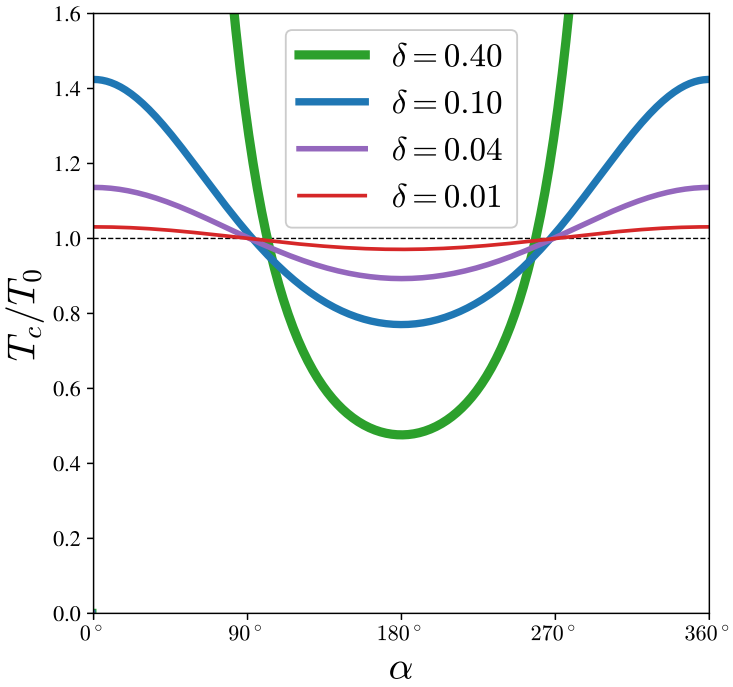

FIG. 2. Normalized orbital period of the chaser as a function of α calculated using Eq. 4. The maximum value of the normalized orbital period for $\delta = 0.40$ is about 125, corresponding to a maximum value of $\epsilon = 0.96$, which shows that this case is approaching an unbound orbit.

for rendezvous, wherein the chaser matches velocities with the target. Obviously, the latter process only occurs when some kind of meeting or docking of the two objects is desired, and would not be applicable in the case of intentional collision, as with the DART mission. Of the two parts, the interception problem is the more difficult, and is the focus of this section. This is because the $\Delta\vec{v}$ that is required for rendezvous is easily found by calculating the difference of the target's velocity and the chaser's velocity, both of which are known once the intercept problem is solved.

The approach to deriving the intercept condition proceeds as follows. Analysis of the radial coordinate is used to determine where the orbits intersect, and therefore the angular locations at which intercept can occur. The angular positions of the target and chaser are then expressed as a function of time. The intercept condition follows by merging these equations to eliminate time and requiring that the target and chaser be at the same angular position, modulo 2π, and at a point of intersection of the orbits.

A. The radial intersection condition

While it is possible to draw an ellipse and a circle that intersect at four locations, the circular and elliptical orbits of the target and chaser can intersect at a maximum of two locations because the chaser's orbit is constrained to have the center of force located at one of its foci, as illustrated in Fig. 1. This is readily proven by requiring the radial position of the chaser (r_c) be equal to that of the target (r_0) and solving for the angular position of the intersection, defined as θ_x. Using the form of r_c given by Eq. 1 and setting $r_c = r_0$ provides the radial intersection condition $\cos(\theta_x + \phi) = \cos(\phi)$, from which two families of solutions emerge. The first is the obvious solution that $\theta_x = 2\pi$, and was the focus of the analysis in Ref. [5]. It appears, based on the image in Fig. 1 that $\theta_x = 2\pi - 2\phi$ defines a second intersection location, at least when $\phi < \pi$. The generalization of the second intersection solution to all angles is

$$\theta_x = \begin{cases} 2\pi - 2\phi & 0 \leq \phi < \pi \\ 4\pi - 2\phi & \pi \leq \phi < 2\pi \end{cases}, \tag{5}$$

where θ_x is limited to the range $[0, 2\pi)$. This expression for θ_x has a sawtooth shape when plotted versus ϕ, and has a curvy-sawtooth function when plotted as a function of α due to the relationship between ϕ and α described by Eq. 3. Both of these forms are shown in Fig. 3. Importantly, the solid orange curves of Fig. 3 will appear in the intercept analysis later.

B. The angular equations of motion

Time dependence enters the description of motion through the angular coordinates. Unlike the Lambert problem where time is an explicit constraint, time is not specified in this problem and will therefore be eliminated by merging the equations of motion for the target and chaser. The target travels on a circular orbit at constant angular velocity ω_0, starting at an initial angle of θ_0, and evolves in time as

$$\theta_t(t) = \theta_0 + \omega_0 t. \tag{6}$$

While the angular position of the target is linear in time, there is no corresponding simple expression for the angular coordinate of the chaser as a function of time. Worse

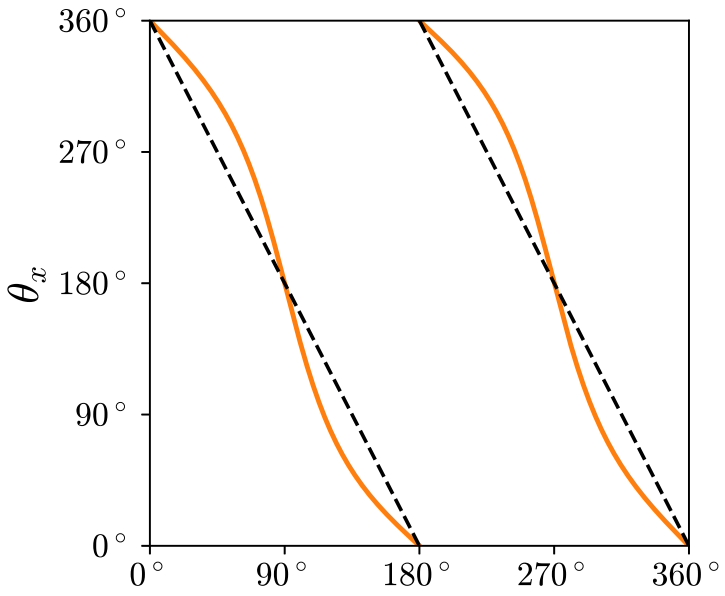

FIG. 3. The intersection angle of the two orbits, θ_x, is plotted against ϕ (black dashed) and α (solid orange) for the case of $\delta = 0.20$. The very weak dependence of ϕ on δ means that the θ_x versus α curves shown here can be taken as representative for a broad range of δ.

yet, an analytic expression is not even possible. However, it is possible to describe the inverse relationship for the chaser, that is, time as a function of angular position. This relationship can be derived from the specific angular momentum equation, $r^2\dot{\theta} = l_c$, by separating variables to get $dt = r_c^2 d\theta / l_c$. Expressing r_c in terms of θ using Eq. 1, and integrating between the initial and final coordinates yields

$$t = T_0 \frac{(1 + \epsilon \cos(\phi))^{3/2}}{2\pi} \int_0^{\theta_c} \frac{d\theta}{(1 + \epsilon \cos(\theta + \phi))^2}, \tag{7}$$

where we have simplified the expression using $\omega_0 = v_0/r_0$ and $l_c = r_0 v_0 (1 + \epsilon \cos(\phi))^{1/2}$, which is an alternate form for l_c that is presented in Eq. A6. Critically, the chaser's angular position now appears as the upper limit of the integral. This result is valid for any final angle of an object and for any values of ϵ and ϕ, which means that parabolic and hyperbolic paths are also potential intercept trajectories given suitable limitations on the final angular position.

For motion involving more than one orbit of the chaser, we can express its angular coordinate as $\theta_c = 2\pi n_c + \theta_c'$, where $n_c \in \mathbb{N}$ counts the number of whole orbits and $\theta_c' \in [0, 2\pi)$.

Looking ahead to the specific problem of intercept, we must limit the final angular position to be at an intersection location of the orbits by setting $\theta_c' = \theta_x$. The time required to travel the total angular distance is then n_c times the orbital period for the whole elliptical orbit, which is given by Eq. 4, plus the remainder described by Eq. 7 evaluated with an upper limit of θ_x. That is,

$$t = n_c T_c + \frac{1}{\omega_0} \left(1 + \epsilon \cos\left(\phi\right)\right)^{3/2} \int_0^{\theta_x} \frac{d\theta}{\left(1 + \epsilon \cos\left(\theta + \phi\right)\right)^2}. \tag{8}$$

Consideration of particular cases requires that the integral be evaluated, which can be accomplished either through direct numerical evaluation or by using an analytic expression for the integral,[3,21,22] which is presented here for the sake of completeness. Defining the second term on the RHS of Eq. 8 as $I\left(\theta_x; \epsilon, \phi\right)/\omega_0$, the analytic expression for this integral is

$$I\left(\theta_x; \epsilon, \phi\right) = \left(\frac{1 + \epsilon \cos\left(\phi\right)}{1 - \epsilon^2}\right)^{3/2} \left[q\left(\theta_x + \phi\right) - q\left(\phi\right)\right], \tag{9}$$

where we have defined a new quantity, q, given by

$$q\left(z\right) = \psi\left(z\right) - \epsilon \sin\Big(\psi\left(z\right)\Big), \tag{10}$$

which itself depends on another quantity ψ, with

$$\psi\left(z\right) = 2 \tan^{-1}\left(\sqrt{\frac{1-\epsilon}{1+\epsilon}} \tan\left(\frac{z}{2}\right)\right). \tag{11}$$

Equations 9–11 are collectively known as Kepler's equation. While simpler than Eq. 8 in that no integral needs to be calculated numerically, Eqs. 9–11 obscure the physical origin of the expression and are rather complicated in their own. When using these equations, care must be taken to enforce continuity in ψ as the inverse tangent function passes from $+\pi/2$ to $\pi/2$, which happens as the argument of the tangent function passes through π. In the following sections, the RHS of Eq. 8 is described using only $I\left(\theta_x; \epsilon, \phi\right)$ so that readers may use their preferred representation of the integral.

C. The intercept condition

The intercept condition is realized when we eliminate time in Eq. 6 by replacing it with the expression for time from Eq. 8 and by imposing the requirement that $\theta_t = \theta_x$ (the

target must also be at a point of intersection of the orbits). Or, since any number of whole orbit motions of the target can be added to its position, the most general statement is $\theta_t = 2\pi n_t + \theta_x$, where $n_t \in \mathbb{N}$. Merging Eqs. 6 and 8, and using the compact expression for the integral in Eq. 8, the generalized intercept condition is given by

$$2\pi n_t + \theta_x \stackrel{!}{=} \theta_0 + n_c \omega_0 T_c + I\left(\theta_x; \epsilon, \phi\right), \tag{12}$$

where the $\stackrel{!}{=}$ symbol is used as a reminder that this is a condition that we want to be true, not one that must be true. It is the rare values of the thrust parameters for which the LHS and RHS of Eq. 12 are equal that define the intercept solutions that we seek.

We briefly pause to consider how Eq. 12 should be interpreted. The origin of this equation is Eq. 6, which describes the angular position of the target as a function of time. The second and third terms on the RHS represent the the time (properly, $\omega_0 t$) required for the chaser to travel to θ_x, an intersection point of the orbits. Therefore, the RHS represents *the actual angular position of the target when the chaser is at* θ_x. The LHS represents *the goal of having the target also at an intersection point.* That this expression is the most general statement of the intercept condition for this problem can be seen by noting that limiting the solution space to $\theta_x = 0$ eliminates the second term on the LHS and the integral term on the RHS, which reproduces the first family of intercept solutions that is described by Eq. 18 of Ref. [5].

IV. SOLUTIONS FOR THE SECOND FAMILY OF INTERCEPT LOCATIONS

This search for intercept solutions proceeds here by taking δ as specified, leaving α as the sole unknown control parameter. Phrased as a question, the intercept condition asks "For what values of α is Eq. 12 true?" Since equation 12 is a transcendental expression given the appearance of θ_x as a linear variable on the LHS and as the upper limit of integration on the RHS (or, equivalently, a variable buried deep in the chain of Eqs. 9–11), solutions will be found by scanning through all possible values of α and identifying solutions as those points for which the LHS and RHS of the intercept condition are equal. In analyzing this problem it must be recalled that θ_x is a function of ϕ through Eq. 5 and that ϵ and ϕ are functions of α and δ through Eqs. 2 and 3, respectively.

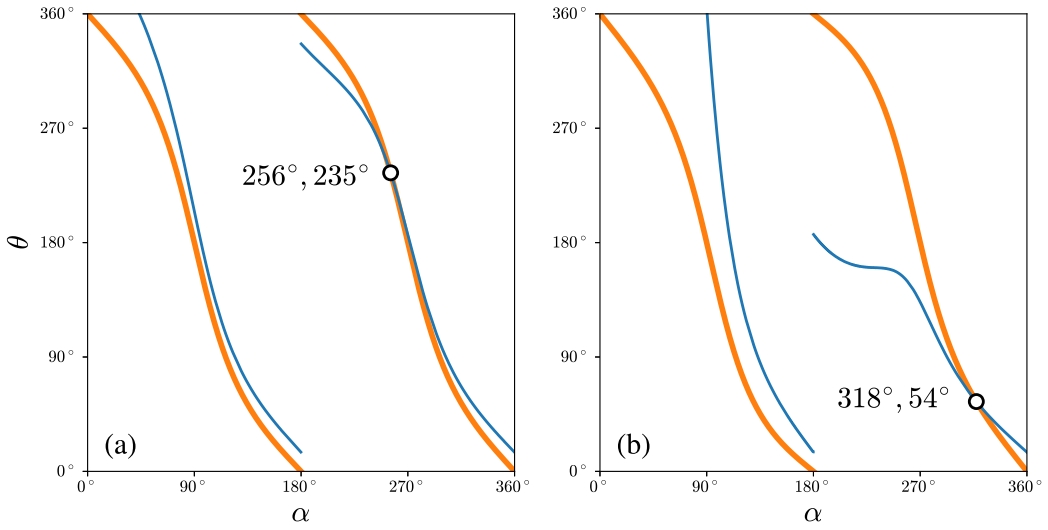

FIG. 4. Calculated as a function of α, the thick orange curves represent the goal of having the target at the intersection location of the orbits and the thin blue curves represent the actual angular position of the target when the chaser is at the intersection location. The crossing of these curves identifies a fast-intercept solution for (a) $\delta = 0.04$ and (b) $\delta = 0.40$. The initial angular separation is $\theta_0 = 15°$ in both cases. The numerical values next to each crossing identify the thrust angle and intercept angle, respectively, that solve the fast-intercept problem.

A. Intercept solutions

Figure 4 presents two fast-intercept solutions ($n_c = n_t = 0$), for $\delta = 0.04$ and $\delta = 0.40$, as representative cases. The second case is close to the normalized Δv limit of $\sqrt{2} - 1 \approx 0.41$ for escape from orbit for a forward thrust and can reasonably be considered a moderate to large thrust. Both cases assume initial conditions where the target leads the chaser (a positive value of θ_0), though it should be noted that there is no reason that this must be so and negative values of θ_0 are perfectly acceptable. The thin blue curves in Fig. 4 represent the RHS of Eq. 12 and should be interpreted as the actual position of the target when the chaser is at a crossing of the orbits (θ_x), which is represented by the thick orange lines. Notably, it seems that these fast-intercept solutions require $\alpha > 180°$, and it is clear that larger values of δ achieve intercept more quickly, findings that are in agreement with the predictions asserted in Section II A. The trajectories for these two fast-intercept solutions are presented in Fig. 5. Notably, the second solution with $\delta = 0.40$ will grossly overshoot the target if there is not a rendezvous maneuver or collision with the target.

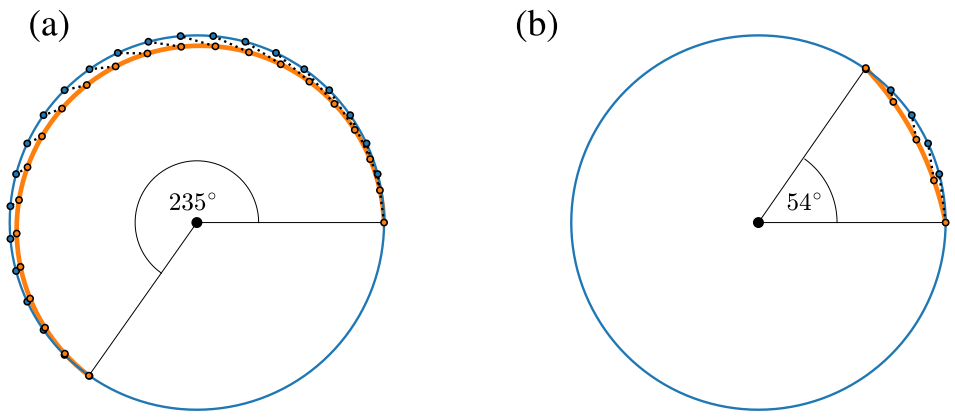

FIG. 5. Strobe-effect illustration of the trajectories of the chaser (orange, thick) and the target (blue, thin), plotted at 10° increments of the target, for the intercept solutions identified in Fig. 4 for (a) $\delta = 0.04$ and (b) $\delta = 0.40$. The black dotted line between the points identifies position pairs at equal intervals of time. The black dots interior to the orbits identify the center of force.

Figure 6 illustrates the solution space for the generalized intercept condition for the case of $\delta = 0.39$ and allowing for multiple orbits of the chaser and target. The value of $\delta = 0.39$ was specifically chosen for its relevance to the sensitivity analysis in the following section. Though the presentation of the intercept condition becomes considerably more complex when considering multiple orbits, the method for identifying solutions remains the same and it is apparent that a wide range of intercept solutions is possible. Table I lists the numerical values for these intercept solutions.

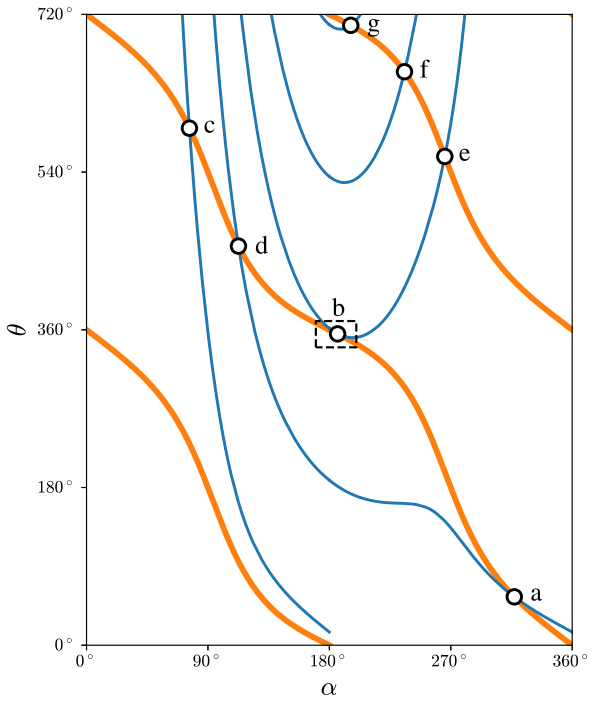

FIG. 6. Intercept curves for $\delta = 0.39$ and $\theta_0 = 15°$ showing all possible solutions for zero and one and orbits of the target. The dashed box indicates the parameter range shown in Fig. 7.

Fig. 6 tag	n_t	n_c	α	θ_x	θ_t	θ_c
a	0	0	317°	56°	56°	56°
b	0	1	186°	355°	355°	715°
c	1	0	76°	230°	590°	230°
d	1	1	113°	95°	455°	455°
e	1	1	266°	198°	558°	558°
f	1	2	236°	295°	655°	1015°
g	1	3	196°	348°	708°	1428°

TABLE I. List of numerical values for the solutions presented in Fig. 6.

V. SENSITIVITY TO VARIATIONS IN α

Trajectory corrections are almost always needed in real missions to compensate for guidance errors, mechanical inaccuracies, and limitations of information and calculation. An efficient and stable trajectory is one where the required corrections are much smaller than

primary mission maneuvers. The Cassini-Huygens mission, for example, was designed with a deep-space maneuver (DSM) Δv of approximately 450 m/s, along with many smaller trajectory correction maneuvers (TCMs), all of which were less than 10% of the primary thrust.[23] The use of small corrections is only possible when the trajectories are relatively stable with respect to errors in the initial thrust vector.

This analysis, like that in Ref. [5], considers the sensitivity to variations in the angular control variable α. A similar analysis could be conducted for variations in δ. With the first family of intercept solutions analyzed in Ref. [5], it was straightforward to show that there exist solutions that are optimally insensitive (stable) because the only dependence on α occurred on the RHS of the first-family intercept condition. The existence of stable solutions for the first family amounted to showing that the derivative of the RHS of the intercept condition with respect to α can be zero for some intercept solutions, which led to the conclusion that forward or reverse thrusts are optimal for the first family of intercept solutions.

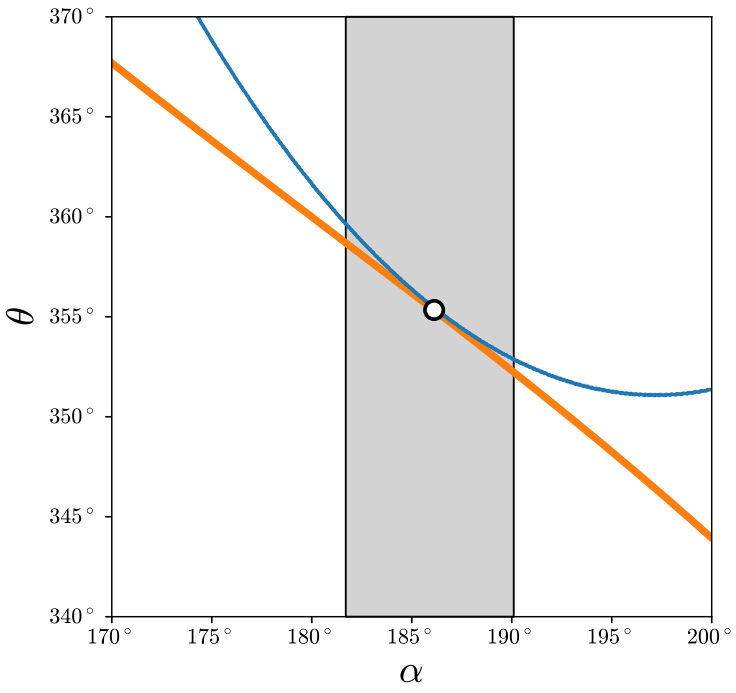

FIG. 7. Intercept solution b identified in the dashed box of Fig. 6. The gray bands identify the range of α for which the target and chaser have an angular separation of 1° or less around the ideal intercept location, which results in an allowable uncertainty on α of about 5°.

An analytic treatment of the sensitivity of the generalized intercept condition is much more difficult on account of the many ways in which both the LHS and RHS of Eq. 12 depend on α. Instead of providing a mathematical proof of the existence of stable solutions, the intercept solutions identified in Fig. 6 are inspected in terms of their sensitivity to small variations in α. In particular, the boxed region in Fig. 6 identifies the region that is expanded in Fig. 7, which shows that the two curves are tangent to each other for intercept solution *b*. Thus, the existence of stable solutions for the generalized intercept condition is proved via example.

Analysis of solution sensitivity to variations in α must also consider the magnitude of the slopes of the curves in the vicinity of the solution. For example, assuming that a mission can tolerate a deviation of 1° between the positions of the craft, analysis of the curves in Fig. 7 shows that the input control can be within of about ±5° of the optimal value of α. Expressed otherwise, an output error of 1° arises from an input error of ±5° for this solution, corresponding to a sensitivity ratio (output variation/input variation) of about 0.2. In contrast, intercept solutions *c*–*g* from Fig. 6 have normalized sensitivities of order 10 and would therefore be unlikely candidates for an intercept mission. Interestingly, solution *a* has an impressive sensitivity ratio of about 0.5 despite the fact that the curves are not tangent at the solution point, a result of the relatively weak gradients in this vicinity. It should be noted that it is possible for low sensitivity solutions to arise even for curves that cross if the crossing occurs at an inflection point of one of the curves, like the solution presented in Fig. 4a.

VI. RENDEZVOUS

The conditions on the thrust required for rendezvous can be derived from the equations of motion or from symmetry arguments, both of which are described here. The chaser's velocity components at interception can be calculated using Eqs. A1 and A2 from the appendix. Evaluating at the intersection angle for the second family of intersection points described by Eq. 5, the azimuthal velocity at interception is $v_{c,\theta} = v_0 + \Delta v \cos(\alpha)$, which is the same as the initial state. Evaluation of the radial component of velocity gives $v_{c,r} = -\Delta v_0 \sin(\alpha)$, which means that the radial velocity at interception is directed opposite to the initial radial velocity. The same conclusion can be surmised from consideration of the motion and the

symmetry of the problem using Fig. 1, where the velocity components must have the same magnitude and the radial component has changed sign. It follows that the rendezvous maneuver at the second family of intercept locations requires a thrust of magnitude Δv at an angle of $\pi - \alpha$.

VII. CONCLUSIONS

The analysis presented in this work concludes the intercept problem that was originally presented in Ref. [5] by demonstrating how the method of solution can be extended to the second family of intersection locations. The constraint of a specified Δv, equivalent to a constraint on fuel, is highly relevant in many contexts and has the benefit that it much easier to visualize a thrust vector that is constant in magnitude and varies only in direction than the more abstract notion of a fixed time to interception that defines the Lambert problem. In addition to presenting a method for finding solutions for the second family of intercept locations, this work has shown how fast-intercept solutions can be calculated. The existence of stable solutions for the second family is proven through an example with $\delta = 0.39$ and $\theta_0 = 15^\circ$.

The intercept condition that is derived here contains both families of intercept solutions and is therefore the most general statement of a solution for this problem. The entirety of this intercept problem, first through the work of Ref. [5] and followed by this analysis, demonstrates how complexity quickly arises as a problem is extended but can nonetheless be greatly simplified when viewed appropriately. In particular, visualizing the solution space as the crossing of curves that represent a trascendental equation is a powerful technique that has applications to many problems in physics and beyond. There are, of course, many other rich and challenging problems that could be further examined using the framework and analytical methods described here, including a mathematical expression for the stability of solutions to the intercept condition, the existence of low-sensitivity fast-intercept maneuvers, initial orbits that are not circular, and initial conditions that are not co-orbital.

AUTHOR DECLARATIONS

The authors have no conflicts to disclose.

---

[1] J. L. Lagrange. *Mécanique Analytique, Vol. II.* Académie des Sciences, Paris, 1788.

[2] C. F. Gauss. *Theory of the motion of the heavenly bodies moving about the Sun in conic sections: a translation of Gauss's "Theoria motus."*. Little, Brown and Co., 1857.

[3] I. R. Gatland. Gravitational orbits and the Lambert problem. *American Journal of Physics*, 90(3):177, 2022.

[4] A. M. Capece and J. L. Gazley. The Hohman transfer as an application for teaching introductory physics. *American Journal of Physics*, 89(11):1002, 2021.

[5] E. M. Edlund. Interception and rendezvous: An intuition-building approach to orbital dynamics. *American Journal of Physics*, 89:559, 2021.

[6] B. W. Carroll. The delicate dance of orbital rendezvous. *American Journal of Physics*, 87(8): 627, 2019.

[7] P. R. Blanco and C. E. Mungan. High-speed escape from a circular orbit. *American Journal of Physics*, 89(1):72, 2021.

[8] L. M. Smallwood, D. M. Katz, and M. W. Richmond. Near earth objects: A brief review and a student project. *American Journal of Physics*, 72(2):264, 2004.

[9] NASA. Planetary defense coordination office, 2022. URL `https://www.nasa.gov/planetarydefense/overview`.

[10] A. F. Chang, A. S. Rivkin, P. Michel, J. Atchison, O. Barnouin, L. Benner, N. L. Chabot, C. Ernst, E. G. Fahnestock, M. Keuppers, P. Pravec, E. Rainey, D. C. Richardson, A. M. Stickle, and C. Thomas. AIDA DART asteroid deflection test: planetary defense and science objectives. *Planetary and Space Science*, 157:104, 2018.

[11] T. Pultarov. Astroscale's space junk removal satellite aces 1st orbital test, 2021. URL `https://www.space.com/astroscale-first-space-junk-capture-demonstration`.

[12] W. J. Hennigan. Exclusive: Strange Russian spacecraft shadowing U.S. spy satellite, general says, 2020. URL `https://time.com/5779315/russian-spacecraft-spy-satellite-space-force/`.

[13] R. D. H. Warburton and J. Wang. Analysis of asymptotic projectile motion with air resistance using the Lambert W function. *American Journal of Physics*, 72:1404, 2004.

[14] B. C. Reed. A guide to the literature of the finite rectangular well. *American Journal of Physics*, 89:529, 2021.

[15] A. A. Othman, M. de Montigny, and F. Marsiglio. The Coulomb potential in quantum mechanics revisited. *American Journal of Physics*, 85:346, 2017.

[16] F. Szmulowicz. Analytical, graphical, and geometric solutions for photonic band gaps. *American Journal of Physics*, 72:1392, 2004.

[17] J. R. Mendonça. Electromagnetic surface wave propagation in a metallic wire and the Lambert W function. *American Journal of Physics*, 87:476, 2019.

[18] E. I. Butikov. Relative motion of orbiting bodies. *American Journal of Physics*, 69(63):63, 2001.

[19] L. J. Rich'e, G. M. Colton, and T. A. Guillory. Apollo 11 flight plan. *NASA*, 1969. URL `https://www.hq.nasa.gov/alsj/a11/a11fltpln_final_reformat.pdf`.

[20] Note1. This referenced NASA report on the Apollo 11 flight plan calls for an initially circular orbit at an altitude of 100 nautical miles, and that the Δv needed for the trans-lunar injection (TLI) maneuver was 10451 feet per second. These values provide an estimate of $\delta \approx 0.409$, assuming an optimal escape maneuver using a forward thrust at $\alpha = 0$.

[21] H. Goldstein, C. P. Poole, and J. Safko. *Classical Mechanics*. Pearson, 2011.

[22] H. D. Curtis. *Orbital Mechanics for Engineering Students*. Elsevier, 2014.

[23] T. Goodson, B. Buffington, Y. Hahn, N. Strange, S. Wagner, and M. Wong. Cassini-Huygens maneuver experience: cruits and arrival at Saturn. *AASI-AIAA Astrodynamics Specialist Conference*, pages Paper AAS 05–286, 2005.

Appendix A: DERIVATION OF THE EQUATIONS FOR ϵ AND ϕ

This derivation of the equations for ϵ and ϕ in terms of the control parameters, δ and α, follows the logic presented in Ref. [5]. Two equations of constraint are developed and merged to derive these key relationships. One constraint emerges from kinematics and angular momentum, and the other from conservation of total energy. At $t = 0$, after the engine burn has been completed, the mass, angular momentum, and total energy of the chaser are constants of the motion. Since any function of these quantities must also be a constant of the motion, the following analysis considers the specific angular momentum and the specific total energy, being the angular momentum and total energy divided by the mass. The specific angular momentum is $l_c = r v_\theta$. Referring to the velocity components described in Fig. 1, it follows that $l_c = r_0\, v_0\, (1 + \delta \cos(\alpha))$ immediately after the engine burn has concluded. This constant of the motion can be used with Eq. 1 to solve for the azimuthal velocity through $v_\theta = l_c/r$, which gives

$$v_{c,\theta} = v_0\big(1 + \delta \cos\big(\alpha\big)\big)\, \frac{1 + \epsilon \cos(\theta_c + \phi)}{1 + \epsilon \cos(\phi)}. \tag{A1}$$

An expression for the radial velocity can be derived using the chain rule on Eq. 1, $v_r = (dr/d\theta)\,\dot{\theta} = (dr/d\theta)\,(v_\theta/r)$, together with the prior result to give

$$v_{c,r} = v_0\big(1 + \delta \cos\big(\alpha\big)\big)\, \frac{\epsilon \sin(\theta_c + \phi)}{1 + \epsilon \cos(\phi)}. \tag{A2}$$

The first constraint is found by taking the ratio of the radial and azimuthal velocities, using Eqs. A2 and A1, and equating this to the ratio of velocities from the initial conditions as depicted in Fig. 1. This yields

$$\frac{\epsilon \sin(\phi)}{1 + \epsilon \cos(\phi)} = \frac{\delta \sin(\alpha)}{1 + \delta \cos(\alpha)}. \tag{A3}$$

The second constraint results from consideration of the specific total energy of the chaser, $e_c = \frac{1}{2}\left(v_{c,r}^2 + v_{c,\theta}^2\right) - GM/r$, which can be calculated using the prior results. Noting that Newton's second law analyzed for the target on its circular orbit gives $GM = r_0 v_0^2$, we have

$$e = \frac{1}{2}\frac{v_0^2}{\big(1 + \epsilon \cos(\phi)\big)^2}\left[\epsilon^2 - 1 + 2\epsilon\Big(\,(1 + \delta \cos(\alpha))^2 - (1 + \epsilon \cos(\phi))\,\Big)\cos(\theta + \phi)\right]. \tag{A4}$$

Equation A4 must actually be independent of angle in order for e to be a constant of the motion. Therefore, the coefficient of the $\cos(\theta + \phi)$ must be identically zero. This yields the second constraint,

$$1 + \epsilon \cos(\phi) = (1 + \delta \cos(\alpha))^2 . \tag{A5}$$

This result also allows the specific angular momentum of the chaser to be expressed as

$$l_c = r_0 v_0 (1 + \epsilon \cos(\phi))^{1/2} . \tag{A6}$$

Finally, the two constraints, Eqs. A3 and A5, can be combined to solve for ϵ and ϕ. These expressions are,

$$\epsilon = \delta \sqrt{\sin^2(\alpha) \left(1 + \delta \cos(\alpha)\right)^2 + \cos^2(\alpha) \left(2 + \delta \cos(\alpha)\right)^2}, \tag{A7}$$

and

$$\tan(\phi) = \tan(\alpha) \frac{1 + \delta \cos(\alpha)}{2 + \delta \cos(\alpha)}. \tag{A8}$$

Useful reference points for characterizing the scale of ϵ are its minimum and maximum values. The minimum of Eq. A7 is $\epsilon = \delta$, which occurs at $\alpha = 90^\circ$ and 270°. A maximum of $\epsilon = \delta(2 + \delta)$ occurs at $\alpha = 0^\circ$ and 180°. It was shown in Ref. [5] that ϕ has very weak dependence on δ, such that the approximation $\tan(\phi) = \frac{1}{2} \tan(\alpha)$ is accurate to within 0.5° for $\delta \leq 0.05$.